Journal of Magnetic Resonance **137,** 10–24 (1999)
Article ID jmre.1998.1637, available online at http://www.idealibrary.com on IDEAL®

Signal Selection in High-Resolution NMR by Pulsed Field Gradients

II. The Design of Gradient Pulse Sequences

David J. Thomas,[1] Lorenz Mitschang,[2] Bernd Simon, and Hartmut Oschkinat[3]

European Molecular Biology Laboratory, Meyerhofstr. 1, Postfach 10.2209, 69012 Heidelberg, Federal Republic of Germany

Received January 21, 1998; revised October 8, 1998

We describe a new and powerful computer program called TRIPLE_GRADIENT which calculates optimized pulsed field gradient sequences for specific coherence pathway selection or rejection. Sequences can be computed for gradient coils acting along one, two, or three perpendicular axes. The program is based on the computational minimization of a penalty function formed from the summed amplitudes of the unwanted signals. The underlying mathematical analysis makes use of a vectorial representation of the way in which a gradient sequence suppresses different signals. It is argued that experiments using well-calculated gradient sequences are quicker and generally perform better than those using extensive phase cycling, especially when suppressing extremely strong solvent signals, and it is shown that in many cases gradient experiments of optimal signal-to-noise ratio can be performed. These claims are illustrated by spectra obtained from an HQQC experiment.

Key Words: **pulsed field gradients; pathway selection; signal suppression; water suppression; HMQ NMR spectroscopy.**

1. INTRODUCTION

A high-resolution NMR experiment is defined by a sequence of radiofrequency (RF) pulses and a procedure for selecting a required set of coherence transfer pathways. Generally speaking, an RF pulse sequence excites an enormous number of coherence transfer pathways. Some of these pathways lead to the signals of interest ("wanted pathways"), which we would hope to be able to detect without interference. Other ("unwanted") pathways must be suppressed so that they do not complicate the spectrum. Phase cycling (*1–3*) is the most commonly applied approach for this purpose, but it has been shown recently that multidimensional NMR spectroscopy can also make use of pulsed field gradients for pathway selection (*4–7, 37*). Gradients induce a position-dependent distribution of the spin isochromates in proportion to the quantum coherence order. We call this effect "dephasing," and its reversal is referred to as "rephasing." Gradient selection can be preferable to phase cycling on account of advantages including reduced measurement times, reduction of t_1 noise (*7*), use of the full range of the analog to digital converter, and improved solvent suppression (*8*). To find optimal gradient sequences is, however, not intuitively easy, especially for the relatively long RF pulse sequences of multidimensional NMR spectroscopy.

In most cases nowadays, a gradient sequence is primarily tuned to rephase the wanted coherence transfer pathways, but there is no guarantee that the unwanted signals are properly suppressed (*9*). Special complications arise when phase-sensitive spectra are required, because it is then necessary to detect simultaneously P- and N-type pathways. This is not a problem when phase cycling is applied. However, if gradients are used, it is often difficult to find gradient sequences that rephase the two types of pathway simultaneously and yet still sufficiently suppress the unwanted ones (*10, 11*).

Mitschang *et al.* addressed these conceptual problems recently by introducing a geometric description of the calculation of gradient sequences (*12*). In principle, field gradients can be applied with arbitrary amplitude in any free precession period within the RF pulse sequence, forming an infinite multitude of potential gradient sequences for the experiment. The geometric formalism allows us to determine a sequence of pulsed field gradients that can rephase as many wanted pathways as possible and also strongly dephase the unwanted pathways. The formalism was originally developed under the assumption that field gradients are applied only along a single spatial direction (normally parallel to the Zeeman field, i.e., a "*Z*-gradient") (*12*). An extension to the case where field gradients can be applied in three mutually orthogonal directions ("*X*-, *Y*-, and *Z*-gradients") is discussed in Part I (*13*). It has been shown that gradient sequences that rephase wanted pathways but strongly dephase unwanted ones can be found in favorable cases by solving an eigenvalue problem (*12*) whose solution tends to specify gradient sequences that suppress the strongest unwanted pathways (i.e., with the largest coherence orders) but

[1] To whom correspondence concerning the program should be addressed.

[2] To whom correspondence concerning the experiments should be addressed, at current address: Columbia University, Department of Chemistry, 3000 Broadway, New York, NY 10027.

[3] Current address: Forschungsinstitut für molekulare Pharmakologie, Alfred-Kowalke-Str. 4, 10315 Berlin-Friedrichsfelde, Federal Republic of Germany.

1090-7807/99 $30.00

may fail to suppress weaker ones. It is difficult to steer the solution of the eigenvalue problem toward gradient sequences that suppress efficiently the most important unwanted pathways. In order to be able to solve the general case routinely and reliably, a numerical procedure is clearly required.

In this paper we present an algorithm built on the geometrical nature of the earlier work (*12, 13*). The calculation of an optimal gradient sequence by solving an eigenvalue problem is abandoned in favor of a direct computational minimization of a realistic estimator of the residual magnitudes of the unwanted signals. The maximum possible amplitude of the field gradients is also taken into account, and different gradient pulses are allowed different durations in order to tailor the gradient sequence realistically for the particular NMR experiment. The corresponding computer program is called "TRIPLE_GRADIENT." It is designed specifically for the optimal implementation and use of field gradients by the experimentalist.

The organization of the paper is as follows: in Section 2, the geometric approach to pathway selection of the earlier work is summarized, as far as it concerns the present work; in Section 3, the algorithm of TRIPLE_GRADIENT is described in the general case when field gradients can be applied along any spatial direction; the details of the mathematics are described in the Appendices; finally, an example in which TRIPLE_GRADIENT is applied to optimize the pathway selection by pulsed field gradients in a $^1H/^{13}C$ correlation experiment is discussed extensively in Section 4. Measured spectra are also presented, demonstrating the rephasing of several and complementary wanted pathways to obtain phase-sensitive spectra in a single scan. Gradients are applied in the evolution period of these experiments.

2. GEOMETRICAL ANALYSIS OF PATHWAY SELECTION

A field gradient exposes a spin system to an inhomogenous magnetic field whose gradient is usually aligned along the otherwise homogenous Zeeman field. We assume that the equipment allows the generation of spatially uniform field gradients along one or more of the three mutually orthogonal directions defined as the conventional laboratory *X*-, *Y*-, and *Z*-axes. As is conventional, we tie our laboratory *Z*-axis to the direction of the Zeeman field. We then define the wavevector

$$\mathbf{k} = \begin{pmatrix} \mathbf{k}_x \\ \mathbf{k}_y \\ \mathbf{k}_z \end{pmatrix} = \gamma \begin{pmatrix} \mathbf{p} \cdot \mathbf{g}^X \\ \mathbf{p} \cdot \mathbf{g}^Y \\ \mathbf{p} \cdot \mathbf{g}^Z \end{pmatrix}, \qquad [2.1]$$

where γ is the gyromagnetic ratio of one of the nuclear species involved in the experiment (*12*) and $\mathbf{p}$ is a vector representing a particular coherence transfer pathway. In the homonuclear case, the *r*th component of $\mathbf{p}$ is the coherence order prevailing in the *r*th period of free precession of the experiment in question (*15*), and in the heteronuclear case this and subsequent equations retain their validity when a so-called composite coherence order is used instead (*12, 15*). $\mathbf{g}^X$, $\mathbf{g}^Y$, and $\mathbf{g}^Z$ are vectors that represent sequences of pulsed field gradients applied along the *X*-, *Y*-, and *Z*-axes, respectively. The *r*th component $\mathbf{g}_r^A = \mathbf{G}_r^A \int_0^{\tau_{0r}} f_r(\tau) d\tau$ is the effective strength or "impact" of a field gradient applied along the specified direction in the *r*th period of free precession, $\mathbf{G}_r^A$ being the amplitude of the field gradient, τ_{0r} its duration, and $f_r(\tau)$ the time profile of the pulse (*13*). $\mathbf{p}$, $\mathbf{g}^X$, $\mathbf{g}^Y$, and $\mathbf{g}^Z$ are vectors in Euclidean spaces isomorphic to and modeled by $\mathbb{R}^F$, where F is the number of periods of free precession of the experiment in question. The radial component of the wavevector is $\mathbf{k}_r = (\mathbf{k}_x^2 + \mathbf{k}_y^2)^{1/2}$. The sample volume affected by a field gradient is taken to be a cylinder of height L and radius R with its center at the origin of the coordinate system and its axis of cylindrical symmetry along the Zeeman field.

The reduction in amplitude of a signal when field gradients are applied (*13*) is given by

$$\sigma(\mathbf{k}) = \sigma(0) \frac{2J_1(\mathbf{k}_r R)}{\mathbf{k}_r R} \frac{\sin(\mathbf{k}_z L)}{\mathbf{k}_z L}, \qquad [2.2]$$

where $J_1(\cdot)$ is the Bessel function of first kind and first order (*14*). Strictly speaking, Eq. [2.2] applies only when the excitation profile of the RF coils is completely uniform within the sample volume, but we do not address further in this work the implied approximation when this assumption fails.

The ultimate attenuation of a pathway depends on the vector argument, $\mathbf{k}$, which appears as the scalar components $\mathbf{k}_r$ and $\mathbf{k}_z$ in Eq. [2.2]. R and L are constants, but $\mathbf{k}$ itself depends on the inner product, Eq. [2.1], which is what makes it possible to interprete the mechanism of pathway selection geometrically. A pathway is rephased (i.e., not perturbed) if $\mathbf{k} = 0$ when field gradients are applied. In this case, the vectors $\mathbf{g}^X$, $\mathbf{g}^Y$, and $\mathbf{g}^Z$ representing the sequences of pulsed field gradients applied along the different directions are orthogonal to the vector $\mathbf{p}$ representing the coherence transfer pathway. For $\mathbf{k} \neq 0$, i.e., if one or several of the vectors $\mathbf{g}^X$, $\mathbf{g}^Y$, and $\mathbf{g}^Z$ are not orthogonal to $\mathbf{p}$, the pathway is dephased and hence attenuated to a certain extent. Generally speaking, the larger the inner product between the pathway and the sequences of field gradients, the greater is the achievable attenuation of the signal because of the way in which Eq. [2.2] falls off.

The overall vector space, $\mathbb{R}^F$, splits naturally and advantageously into three parts (*13*). The first is the subspace spanned by the wanted pathways, and is hence called "selective." The remaining part of $\mathbb{R}^F$ is decomposed into two further parts. The suppressive subspace comprises the components of the unwanted pathways outside of the selective subspace, whilst the free subspace is any remaining part of $\mathbb{R}^F$ that can be spanned neither by a wanted nor by an unwanted pathway.

The condition that a gradient sequence not perturb the

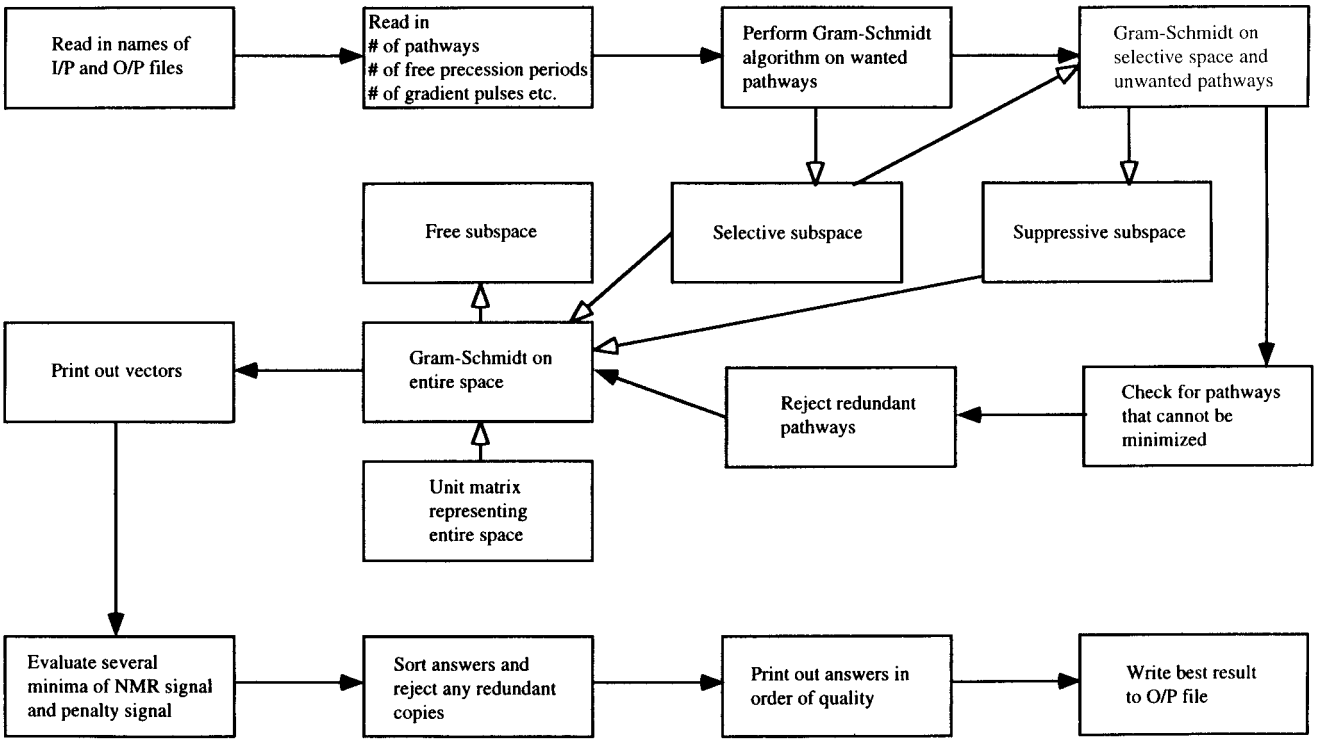

FIG. 1. Flow chart of the TRIPLE_GRADIENT program. The arrows with filled heads denote passage of program control. The arrows with open heads denote flow of data.

wanted signals can now be met simply by generating it from within the suppressive and free subspaces, and avoiding the selective one. The suppression of unwanted pathways depends entirely on components from the suppressive subspace, and any adjustments of the sequence to accommodate instrumental limitations are controlled by admixture of components from the free subspace. Optimization proceeds by the route of minimizing the sum of the amplitude of all unwanted signals (so that the worst receive the most attention) plus a smooth penalty function describing instrumental limitations.

3. THE ALGORITHM

A flow-chart diagram of the successive computational steps in TRIPLE_GRADIENT is shown as Fig. 1. The algorithm (described in detail in this section and in the appendices) uses directly the geometrical analysis outlined in the preceding section.

TRIPLE_GRADIENT reads as input a list of all excited coherence transfer pathways that are considered to be important. Each pathway is coded as an array of F real numbers which are the respective coherence orders of the specified pathway prevailing in the F free precession periods of the experiment. The user must specify which pathways are wanted and which unwanted. In principle, field gradients may be applied in any of the F periods of free precession, but this is sometimes not desirable, and certain periods are better excluded, e.g., very short periods or periods in which a field gradient might interfere with RF decoupling pulses. TRIPLE_GRADIENT therefore allows the user to specify which periods of free precession to use. The duration of each gradient pulse must also be specified (in milliseconds). This makes it possible to maximize the overall strength of a gradient sequence, since different gradient pulses can be adapted to the timing of the RF pulse sequence. On some spectrometers it is possible to vary the time profiles of the gradient pulses, but the program currently assumes the use of rectangular ones. The number of periods of free precession allowed to contain a gradient pulse defines the dimension of the entire space (i.e., $\mathbb{R}^F$ when all periods of free precession are allowed) which is later decomposed into the three subspaces. The choice of periods of free precession in which field gradients might be applied is therefore a crucial step in the procedure, as will be outlined in Section 4 by several examples. In the subsequent calculations within TRIPLE_GRADIENT, the pathway vectors of the input file are reduced to components corresponding to the user's choice of periods of free precession.

The next steps are the explicit calculation of the selective, suppressive, and free subspaces by repeated application of the Gram–Schmidt procedure (*16*) (see Fig. 2). Specifically, the selective subspace is generated by applying the Gram–Schmidt algorithm to the set of all wanted pathways. The suppressive

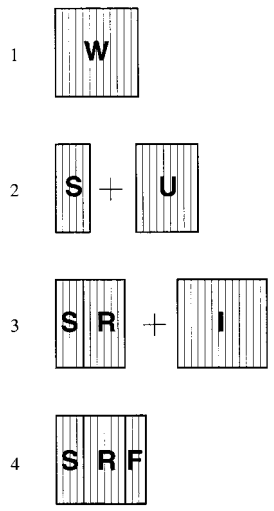

FIG. 2. The vector spaces subjected to the Gram–Schmidt algorithm. The set of vectors representing wanted pathways are shown diagrammatically as a usually nonsquare matrix *W* in row 1. This set is fed as input to the Gram–Schmidt algorithm, which outputs a usually smaller matrix *S* representing the selective subspace in rows 2, 3, and 4. Once calculated, *S* is held fixed. Then the set of unwanted pathways is assembled into a matrix *U* and appended to *S* (row 2). The combined pair are again fed as input to the Gram–Schmidt algorithm, and the result is the generally nonsquare matrix *SR*, *S* being as before, and *R* being the suppressive subspace (row 3). Like *S*, *R* is not allowed to change once it is calculated. Finally, the unit matrix, representing the full space, is appended to *SR* and the entire matrix subjected to the Gram–Schmidt algorithm a third and final time. This time *I* is reduced to *F*, representing any remaining free subspace (row 4).

subspace is then generated by applying the Gram–Schmidt algorithm both to the selective subspace (now held fixed) and to the unwanted pathways. Finally, a unit matrix (representing the entire space) is appended to both the selective and suppressive subspaces and the Gram–Schmidt algorithm is applied a third time (both the selective and suppressive subspaces now being held fixed). Any surviving vectors define the free subspace. The program issues warning messages for any unwanted pathways that lie in the selective subspace since they have no component along the suppressive subspace, making it impossible to find an appropriate gradient sequence. Such unwanted pathways are excluded from further calculation.

Any gradient sequence that rephases all wanted pathways is represented by a vector within the suppressive and free subspaces (i.e., the entire space excluding the selective space), and correspondingly any vector within this common space corresponds to a gradient sequence that rephases all wanted pathways. The next computations in TRIPLE_GRADIENT are to calculate the most efficient gradient sequences, i.e., those that most effectively minimize the residual signals from unwanted pathways. The sequence is represented as a linear combination of the base vectors of the suppressive and free subspace as obtained by the Gram–Schmidt algorithm described above. Thus, the actual free parameters are the linear coefficients. These are varied independently to minimize a suitable penalty function representing residual unwanted signals.

The construction of a penalty function starts from Eq. [2.2]. Ideally, Eq. [2.2] would be a good description of the decay of a single unwanted pathway, but in practice neither the requirement for constant gradients nor that for uniform excitation by the RF pulses is satisfied, and Eq. [2.2] must be regarded as an approximation. Experiments (not presented) have also confirmed that it is not feasible to adjust conditions in order to work at a zero-crossing point of Eq. [2.2]. The best strategy, therefore, seems to be the simple one of maximizing the arguments $\mathbf{k}_r$ and $\mathbf{k}_z$. This works because the envelope of the (oscillatory) function $\sin(v)/v = \mathrm{sinc}(v)$ falls as $1/|v|$, and the envelope of the (oscillatory) function $2J_1(v)/v$ falls approximately as $\pi/2|v|^{-3/2}$ (*14*). Following this reasoning, the attenuation of a single pathway is monitored by fitting an envelope function to Eq. [2.2]. The envelope of the sinc function is represented accurately by a specifically constructed function called sincenv, and the envelope of the function $2J_1(v)/v$ is approximated to more than adequate accuracy by a similarly constructed function, Bessenv. The construction of these envelope functions is discussed in greater detail in Appendix A1. The penalty function actually minimized must take into account the residual signals of all unwanted pathways, which we write as

$$N = \sum w\ \mathrm{Bessenv}(\mathbf{k}_r R)\mathrm{sincenv}(\mathbf{k}_z L). \qquad [3.1]$$

The weights *w* can be set by the user and can represent the various expected amplitudes of different signals, but can equally be set to other values to express varying experimental emphases. As described above, each of the sequences of pulsed field gradients applied along the *X*-, *Y*-, or *Z*-axes is represented by a linear combination of the base vectors of the suppressive and the free subspace. These linear coefficients enter as free parameters the penalty function via its argument, **k** (defined in Eq. [2.1]), together with the components along the suppressive subspace of the unwanted pathways. Equation [3.1] adopts its minimum for the gradient sequences that simultaneously rephase all wanted pathways while maximally dephasing the unwanted ones.

As it stands, the response signal above can be decreased without limit by increasing the strengths of the field gradient pulses. Real gradients are limited, however, and it is also not necessarily desirable to use the maximum values available, for example because of fears of nonlinearity, massive eddy currents, and other possible problems. For this reason, TRIPLE_GRADIENT also includes a penalty function that rises smoothly to infinity as each gradient pulse approaches a prescribed limit. This function has the form

$$P = \sum_r \frac{c\hat{\mathbf{g}}^4}{2(\hat{\mathbf{g}}^2 - \mathbf{g}_r^2)}, \qquad [3.2]$$

where $\hat{\mathbf{g}}$ is the maximum permitted strength of a gradient pulse, and $\mathbf{g}_r$ represents the strength of a single gradient pulse applied in the rth period of free precession. $\hat{\mathbf{g}}$ is calculated as the integral of the time profile of the specified pulse over its duration multiplied by the maximum possible amplitude of the field gradient. We set the latter to 50 G cm^{-1} for longitudinal gradient pulses, and to 35 G cm^{-1} for the transverse ones, though these values are installation-dependent. The specific form of the limiting function is dictated by the requirement that the curvatures at the origin have uniform controllable values to minimize any perturbation to the normal running of the minimization routine in this region. The contours of this instrumental penalty function are isotropic (i.e., circular, spherical, hyperspherical, etc.) near the origin if c is the same for all pulses in the sequence, but they blend smoothly into a rectangular shape as the instrumental limits are approached (a similar function has been used before in a different application (*29*)). This means that when degrees of freedom exist (i.e., there is a free subspace), the overall profile of the pulse sequence may be altered to make maximal use of the instrumental capabilities.

As with any minimization problem, care must be taken to avoid the possibility of becoming trapped in a local minimum and thus failing to find a better solution. Our resolution of this problem has been to restart the minimization a specified number of times (usually 16 for a single gradient, and 64 for a triple-gradient probe) and then to select the best result. It often happens that results are coincident, and the program includes code to reject the redundant solutions.

At the end of a run, TRIPLE_GRADIENT provides the following information. The base vectors of the selective, suppressive, and free subspaces are listed with an indication of unwanted pathways that lie in the selective subspace and are therefore not subject to minimization. The limiting strengths, $\hat{\mathbf{g}}$, are given for the different pulses along all three directions (in ms G cm^{-1}). The best solution of the different trials of minimization, i.e., the optimal sequences of pulsed field gradients ($\mathbf{g}^X$, $\mathbf{g}^Y$, and $\mathbf{g}^Z$), along the X-, Y-, and Z-axes is printed out. The strength (in ms G cm^{-1}) and duration (in ms) of each pulse, the latter as set by the user, and its calculated amplitude (in G cm^{-1}) are also printed out. Strength and amplitude both carry a sign to indicate the relative direction of the field gradients. It may be that in a given solution $\mathbf{g}^X$, $\mathbf{g}^Y$, and $\mathbf{g}^Z$ are identical apart from scale, as discussed in Part I (*13*). In this case, the application of any of these sequences alone will yield qualitatively the same result. To identify these cases, the vectors representing the best solution are shown a second time, but normalized to unit length, and their inner products are calculated. Results near to ± 1 indicate equivalent gradient sequences. Finally, all unwanted coherence transfer pathways are listed with their residual amplitudes if the best solution is used.

The simultaneous application of two or three identical sequences would be expected to result in better suppression, but when the suppression is already very good, further improvements are generally not forthcoming in practice because of nonlinear effects not included in the calculations.

4. EXAMPLE AND RESULTS

TRIPLE_GRADIENT calculates optimized gradient sequences for the pathway selection problem specified in its input file. The user defines whether a specific pathway is wanted or not and at which positions in the RF pulse sequence a field gradient can be applied. It is therefore the user's task to find requirements appropriate for a well-executed experiment. The crux is the distribution of the pathways with respect to the selective and suppressive subspaces. For a given choice of free precession periods, the selective and suppressive subspace form a common space of fixed size, being the space spanned by all pathways. In general, the higher the number of wanted pathways, the larger will be the selective space, and the smaller the suppressive subspace. In some cases it may even be that no freedom remains, and it may no longer be possible to suppress some important pathways (see Part I (*13*)). On the other hand, for a given set of wanted and unwanted pathways, the number of unwanted pathways with a component outside the selective space depends on the choice of free precession periods, and it can be important to make this choice in a way that maximizes the dimension of the suppressive subspace. Clearly, this dimension will be at its largest when all possible free precession periods are used. It is, however, generally desirable to switch as few gradient pulses as possible, particularly for inviscid samples, in order to minimize signal loss from translational diffusion (*31*). In this particular case, it is also preferable that the gradient pulses be applied in neighboring free precession periods. Use of TRIPLE_GRADIENT therefore proceeds in two steps: first, the best set of wanted and unwanted pathways is evaluated, usually allowing all periods of free precession to be used; second, any gradient pulses that are not strictly required are eliminated. These methods are illustrated for the signal selection using the heteronuclear quadruple quantum coherence (HQQC) correlation technique (*17, 18, 30*). The pulse sequence of this experiment and the pathways to be selected are shown in Fig. 3. The key element of the experiment is the generation of HQQC at the beginning of t_1, which is then typically utilized as a filter for CH_3 groups. The standard technique, however, suffers the disadvantage of needing no fewer than 24 steps of phase cycling to select the CH_3 signals properly. Signal selection in the HQQC experiment has been treated before by solving an eigenvalue problem: it was possible to calculate a sequence of pulsed field gradients which attenuated all of the unwanted pathways but it rephased only two of the eight wanted pathways (*12*). These two pathways are of the same P-type, so the spectra had to be processed as absolute values (*19*). We have used TRIPLE_GRADIENT to reexamine the pathway selection in this HQQC experiment. The aim was to find a different pulsed field gradient sequence to rephase more than two wanted pathways, and thus enhance

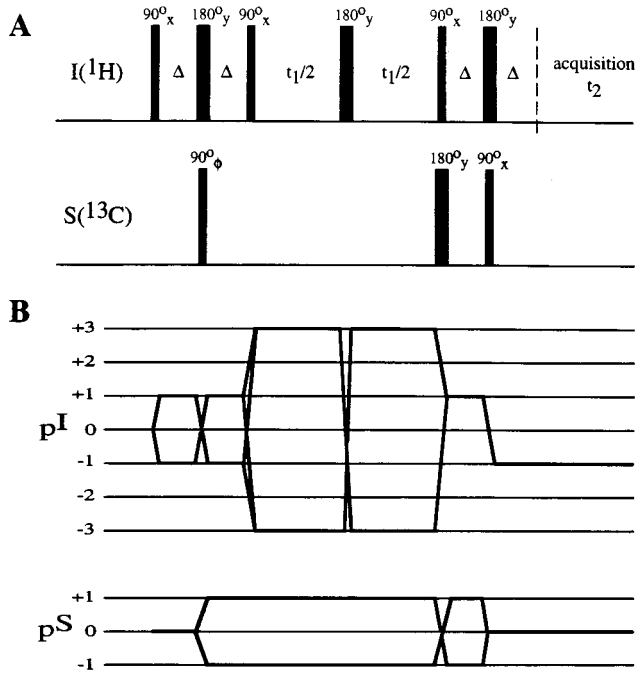

FIG. 3. (A) Pulse sequence for 2D heteronuclear quadruple quantum NMR spectroscopy. (B) Pathways to be selected in our demonstration experiment.

the signal-to-noise ratio. In particular, we wanted to rephase both P- and N-type signals simultaneously so that pure-phase spectra can be obtained in a single scan (*19*).

All detectable coherence transfer pathways that might be excited with a typical protein sample during this HQQC experiment are listed in Table 1. It is assumed that heteronuclear coherences of CH, CH_2, and CH_3 groups and homonuclear proton coherences of orders up to ± 3 (for hydrogens not bound to ^{13}C) are created. Pathways induced by possible imperfections of the RF pulses are not taken into account. Each row in Table I is a vector of six components, representing a certain coherence transfer pathway. The *r*th component of this vector (in the *r*th column of Table 1) is the composite coherence order of the specified pathway prevailing in the *r*th period of free precession (*12, 15*). Each pathway ends with a composite coherence order of -1, because quadrature detection is applied to the protons. The first 8 vectors of Table 1 represent the 8 pathways of the HQQC experiment that contribute to the CH_3 signals. Apart from these 8 wanted pathways, there are 34 unwanted ones originating from carbon–proton correlations of multiplicities other than 3, or from homonuclear proton correlations.

All 34 unwanted pathways must be properly suppressed for a proper signal selection in this HQQC experiment, regardless of whether phase cycles or pulsed field gradients are used.

In an HQQC experiment where the signal selection is done by a phase cycle of 24 steps, all 8 wanted pathways can indeed be retained, and all 34 unwanted pathways can also be suppressed. The resonances in the 2D spectrum have maximal intensity and pure absorption phase, because 4 wanted pathways of P-type are balanced by the 4 remaining N-type wanted pathways. The notions P-type and N-type refer to the coherence order of the carbons being $+1$ or -1, respectively, since the proton chemical shifts of the HQQC prevailing in t_1 are rephased by a π-pulse. Viewed as composite coherence order, carbon coherence order is weighted by $(\gamma_C/\gamma_H) \approx 0.25$, and P- and N-type signals are indicated by the numbers $+0.25$ and -0.25, respectively (*12, 15*).

TABLE 1
Improved Gradient Pulse Sequences

Pathway number	Composite coherence orders in given free precession periods					
	1	2	3	4	5	6
1	1	−0.75	3.25	−2.75	0.75	−1
2	−1	1.25	3.25	−2.75	0.75	−1
3	1	−0.75	−2.75	3.25	0.75	−1
4	−1	1.25	−2.75	3.25	0.75	−1
5	1	−1.25	2.75	−3.25	1.25	−1
6	−1	0.75	2.75	−3.25	1.25	−1
7	1	−1.25	−3.25	2.75	1.25	−1
8	−1	0.75	−3.25	2.75	1.25	−1
9	1	−1	0	0	1	−1
10	−1	1	0	0	1	−1
11	1	−1	1	−1	1	−1
12	−1	1	1	−1	1	−1
13	1	−1	2	−2	1	−1
14	−1	1	2	−2	1	−1
15	1	−1	3	−3	1	−1
16	−1	1	3	−3	1	−1
17	1	−1	−1	1	1	−1
18	−1	1	−1	1	1	−1
19	1	−1	−2	2	1	−1
20	−1	1	−2	2	1	−1
21	1	−1	−3	3	1	−1
22	−1	1	−3	3	1	−1
23	1	−0.75	2.25	−1.75	0.75	−1
24	−1	1.25	2.25	−1.75	0.75	−1
25	1	−0.75	−1.75	2.25	0.75	−1
26	−1	1.25	−1.75	2.25	0.75	−1
27	1	−1.25	1.75	−2.25	1.25	−1
28	−1	0.75	1.75	−2.25	1.25	−1
29	1	−1.25	−2.25	1.75	1.25	−1
30	−1	0.75	−2.25	1.75	1.25	−1
31	1	−0.75	1.25	−0.75	0.75	−1
32	−1	1.25	1.25	−0.75	0.75	−1
33	1	−0.75	−0.75	1.25	0.75	−1
34	−1	1.25	−0.75	1.25	0.75	−1
35	1	−1.25	0.75	−1.25	1.25	−1
36	−1	0.75	0.75	−1.25	1.25	−1
37	1	−1.25	−1.25	0.75	1.25	−1
38	−1	0.75	−1.25	0.75	1.25	−1
39	1	−0.75	0.25	0.25	0.75	−1
40	−1	1.25	0.25	0.25	0.75	−1
41	1	−1.25	−0.25	−0.25	1.25	−1
42	−1	0.75	−0.25	−0.25	1.25	−1

TABLE 2
Improved Gradient Pulse Sequences

Wanted pathways	Periods of free precession	Dimensions			Refocused unwanted pathways	Optimal gradient pulses	Penalty
		Sel.	Sup.	Free			
All (1–8)	all (1–6)	4	0	2	All (9–42)	—	—
Any 7	all (1–6)	4	0	2	All (9–42)	—	—
Any 6	all (1–6)	4	0	2	All (9–42)	—	—
Any 5	all (1–6)	4	0	2	All (9–42)	—	—
1–4	all (1–6)	3	1	2	15–18, 23–26, 31, 32	(29.0, 29.0, 34.8, 34.8, −34.8, −1.4)	0.015
5–8	all (1–6)	3	1	2	19–22, 27–30, 33, 34	(30.5, 30.5, 36.0, 36.0, −8.0, −35.6)	0.018
1, 2, 5, 6	all (1–6)	3	1	2	15, 16	(10.2, 10.2, 0.7, 24.9, 35.8, −36.8)	0.014
	1, 2, 4–6	3	1	1	15, 16	(11.6, 11.6, 0.0, 24.2, 35.8, −36.8)	0.014
	3–6	2	1	1	15, 16	(0.0, 0.0, 5.6, 29.6, 35.1, −36.8)	0.014
→	4–6	2	1	0	15, 16	(0.0, 0.0, 0.0, 20.0, 20.0, −40.0)	0.017
1, 5	all (1–6)	2	2	2	15	(−3.5, 15.1, 1.5, 19.8, 36.5, −37.0)	0.016
	1, 2, 4–6	2	2	1	15	(−0.5, 18.0, 0.0, 18.3, 36.3, −37.1)	0.016
→	2, 4–6	2	2	0	15	(0.0, 18.0, 0.0, 18.0, 36.0, −36.0)	0.016
1	all (1–6)	1	3	2	—	(15.3, 1.2, 21.4, 7.2, −37.2, 36.4)	0.017
	2, 4–6	1	3	0	—	(0.0, −28.0, 0.0, 31.8, 36.6, −38.9)	0.025
→	3–6	1	2	1	2	(0.0, 0.0, 28.0, 10.0, −40.0, 33.5)	0.017

If the goal of selecting all 8 wanted pathways and suppressing all 34 unwanted ones could be achieved with pulsed field gradients, the HQQC experiment could be done in a single scan and would yield a pure-phase spectrum. However, rephasing the 8 vectors of Table 1 necessarily also rephases all 34 unwanted pathways, meaning that pulsed field gradients cannot achieve the same results as phase cycling in this case. In order to select signals from the CH_3 groups, it is therefore necessary to select fewer wanted pathways to allow a suppressive subspace to arise. Various choices for the HQQC experiment are summarized in Table 2. It can be seen that it is necessary to halve the number of wanted pathways. These results are in complete agreement with the discussions in Part I (*13*). Further, to obtain a phase-sensitive spectrum, only certain combinations of wanted pathways can be allowed. One possibility is to acquire two datasets by repeating the experiment, the first for P-type pathways and the second for N-type. The datasets can then be coprocessed to obtain the phase-sensitive spectrum (*10*). In the HQQC experiment, four of the pathways that code for CH_3 signals are P-type (being the first four pathways in Table 1), and the remaining four are N-type. A gradient sequence designed to rephase only P-type pathways must treat the N-type pathways as unwanted. The results of calculations with TRIPLE_GRADIENT for this problem (using all periods of free precession) are summarized in line 5 of Table 2. If four pathways coding for CH_3 signals are classified as wanted, the dimensionality of the selective subspace reduces from 4 to 3, and a new one-dimensional suppressive subspace arises. It is therefore possible to calculate a gradient sequence to suppress unwanted pathways having a component along this one-dimensional subspace. However, some of the unwanted pathways lie within the selective subspace spanned by the four wanted P-type pathways, and must therefore be rephased (column 4 of Table 2). Pathways {15 . . . 18} code for homonuclear proton coherence, whose signals should show up as axial peaks in the spectrum and can be suppressed by a two-step phase cycle. The rephased unwanted pathways {23 . . . 26, 31, 32} code for signals from CH and CH_2 groups. The suppression of these peaks is essential for the selection of CH_3 groups in the HQQC experiment, which would otherwise require a further six-step phase cycle. Similar results are obtained when trying to select only N-type pathways (see line 6 of Table 2) so this scheme of trying to obtain P- and N-type data with field gradients is no improvement on an HQQC experiment in which only phase cycling is used.

A second approach to obtain phase-sensitive spectra is to apply gradient sequences that rephase P- and N-type pathways simultaneously. In the HQQC experiment, P-type pathways {1, 2} combine with N-type pathways {5, 6} to give pure absorption lineshapes. The results of calculations by TRIPLE_GRADIENT when pathways {1, 2, 5, 6} are classified as the wanted ones, and pathways {3, 4, 7, 8, 9 . . . 42} are unwanted, is shown as line 7 of Table II. When all periods of free precession are taken into account, the selective subspace is three-dimensional and the suppressive subspace is one-dimensional, exactly as in the case when only P- or N-type pathways are wanted (lines 5 and 6 of Table 2). However, only 2 of the 38 unwanted pathways are in the selective subspace, and will therefore necessarily be rephased. Pathways {15, 16} both code for homonuclear (proton) triple quantum coherence and are not expected to be excited to any great extent in the HQQC experiment. The corresponding peaks are axial and can be suppressed with a two-step phase cycle. This scheme of pathway selection seems to be a definite improvement: the exten-

sive phase cycle is no longer needed, and the spectra can be acquired in the phase-sensitive mode. However, only half of the CH_3-group pathways are detected, so the signal intensity is only half of that obtained from the phase-cycled HQQC experiment. When all periods of free precession are taken into account, the solution calculated by TRIPLE_GRADIENT sets a gradient pulse in every interval of the RF sequence. As indicated in Table II, it is actually possible to obtain the same pathway selection with fewer gradient pulses: three pulses, applied in the last three periods of free precession, are sufficient for the signal selection. If the first of these gradients is switched in the evolution period of the HQQC experiment, a pure absorption lineshape can be obtained in a single scan.

It is possible to prevent the rephasing of any undesired pathway by reducing the number of wanted pathways even further. If the P-type pathway {1} and the complementary N-type pathway {5} are the two wanted pathways, only the unwanted pathway {15} will be rephased in addition (see line 8 of Table II). Line 9 of Table II shows the case of a single wanted pathway, e.g., {1}: TRIPLE_GRADIENT has calculated gradient sequences to suppress all other pathways. One extra pathway amongst the 41 undesired ones, namely pathway {2}, is rephased together with the wanted one if gradients are used in the last four free precession periods of the HQQC experiment. Pathway {2} is degenerate with the wanted pathway with regard to these periods, but being rephased causes no problem because it is one of the eight CH_3-group pathways. The signal intensity consequently doubles.

Optimal gradient sequences for different pathway selections are presented in Table 2. The calculations were performed on the basis that all gradient pulses are assumed to have a rectangular time profile and a duration of 1 ms. All unwanted pathways were given the same penalty function (i.e., $w = 1$ in Eq. [3.1]). The penalties in Table 2 are the value of the penalty function evaluated for each solution. For the pathway selection shown arrowed in the seventh row of Table 2, the penalty is 0.017, for example. According to the calculation, 36 unwanted pathways are attenuated by the indicated gradient sequence and the average residual of the suppressed pathways is $\sim$0.0005. The output from TRIPLE_GRADIENT lists the residual amplitudes of all unwanted pathways.

We used the gradient sequences shown arrowed in Table 2 for HQQC experiments at 290K on a sample of cyclosporin A in perdeuterated dimethyl sulfoxide (DMSO). This cyclic peptide has 16 conformations in DMSO, of which 8 are significantly populated, so 8×24 methyl groups should appear, counting all of the groups in the amino-acid side chains and in methylated peptide bonds. The sample was not isotopically labeled, so the unwanted pathways from homonuclear proton coherence (pathways {9 . . . 22} in Table 1) are a hundred times stronger than the wanted pathways because of the low natural abundance of ^{13}C. To facilitate a complete suppression of these pathways, a 2-step phase cycle on the first ^{13}C RF pulse and on the receiver is used in all experiments together with the gradient pulses. This phase cycle also suppresses the unwanted pathways {15, 16}, which are rephased by some of the gradient sequences.

To compare the intensities of the signals, 1D spectra were acquired with the RF pulse sequence of Fig. 3. The spectra in Fig. 4 were obtained from experiments in which gradient sequences corresponding to the three shown arrowed in Table 2 are applied in conjunction with a two-step phase cycle as described above. Figure 4C shows the signals when pathways {1, 2, 5, 6} are rephased. The signals in Fig. 4B are from pathways {1, 5}, and those in Fig. 4A from pathways {1, 2}. The intensities reflect the number of rephased pathways. Despite the fact that the signals are less intense than in the phase cycled experiment, the spectra are of a higher quality and have a better signal-to-noise ratio. It should be noted that signals subtracted in the phase-cycle experiment have an intensity 100 times greater than do the signals of interest, and subtraction errors may cause a high residual noise. In experiments using gradients, signals that are further suppressed by the two-step phase cycle are much reduced in intensity.

5. DISCUSSION

Gradient selection of coherence transfer pathways must meet several practical requirements to be useful for routine NMR spectroscopy. Most importantly, the gradient sequences themselves should guarantee that the actual NMR experiment is the one required, in the sense of ensuring the capture of the wanted signals and the simultaneous suppression of the unwanted ones. This should be done without deleterious consequences such as a loss in signal-to-noise ratio caused by an inability to rephase some of the wanted pathways. Further, the gradient sequences are best chosen so that it is easy to obtain pure-phase spectra in the indirect dimensions without introducing artifacts. The ability to suppress selected strong resonances with specially tuned gradient sequences is of similar importance and offers the possibility of avoiding the strong t_1 noise that tends to occur with phase cycling. The TRIPLE_GRADIENT program is designed to offer facilities to match these criteria as fully as possible, and is specifically helpful for trying to design gradient sequences to suppress many unwanted pathways while simultaneously rephasing wanted pathways to obtain pure-phase spectra. The number and kind of pathways to be selected or suppressed are chosen by the spectroscopist, and TRIPLE_GRADIENT then determines whether or not any appropriate gradient sequences exist. The program can also be used iteratively, as described in the Results section, where an optimal answer to particularly difficult problems can be found by successively trading off phased and dephased pathways. For practical applications it should be the ratio of the field gradients that is kept as the main result. The maximal strength of the largest gradient in the calculated sequence should then be chosen so that experimental problems such as eddy currents and gradient nonlinearities are minimized. In cases where the

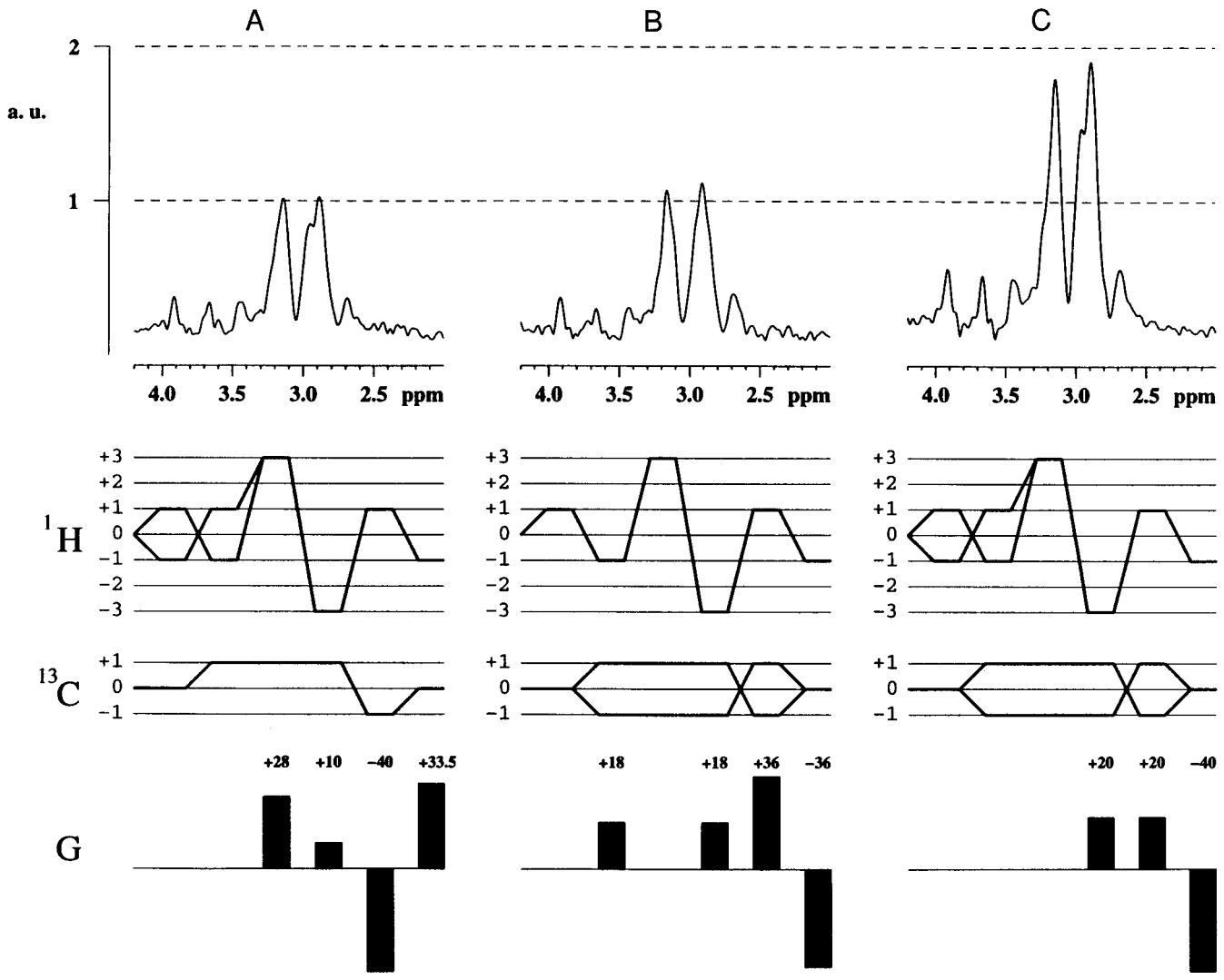

FIG. 4. Observed spectra. Upper row: 1D HQQC spectra of cyclosporin in DMSO solution at 290 K. Only the region comprising the *N*-methyl groups is shown. Middle row: selected pathways used for generating the spectra above. Lower row: gradient sequences used for pathway selection. The pathways in the middle and right columns yield pure-phase data.

calculated gradient sequence along all three gradient axes is the same, which is true for most of the cases we have calculated so far, we recommend the application of the gradient sequence at the magic angle, when a strong solvent signal is present. This avoids artifacts arising from local dipolar demagnetization fields (*32–36*).

The algorithm described in this paper is quite different from its forerunner, which reformulated the minimization procedure as an eigenvalue problem. This had the undesirable consequence of dominantly suppressing pathways that were easy to suppress, and failing to suppress adequately those that were less easy to suppress. The new program concentrates its efforts more evenly. Indeed, it should be noted that the example chosen in the Results section could be solved only with the new program, which explores more thoroughly the space of wanted and unwanted coherence pathways. The new program minimizes contributions from different pathways explicitly, and each can be weighted individually, neither of which was the case with the old. For the HQQC sequence used as an example in this paper, the new program allowed us to select several coherence transfer pathways at the same time, while retaining a pure-phase spectrum. We expect TRIPLE_GRADIENT to give experienced spectroscopists the chance to reconsider the application of pulsed field gradients in many commonly used pulse sequences and to obtain spectra of optimal signal-to-noise ratio and phase properties.

APPENDIX A1

Approximations to Envelope Functions

A major difference between the present and earlier work [12] is the use of envelope functions to describe the general

decay of the functions sinc and $2J_1(v)/v$. The sinc(v) function is the easier to deal with because the envelope away from the central maximum has an exactly known form, namely $1/|v|$. This diverges as $|v| \rightarrow 0$, grossly misrepresenting the true envelope in this region. It is therefore necessary to find a function that properly represents the sinc function near the origin and also osculates with $1/|v|$ at some suitable blend point (we use $v = \pi$, though the precise value is not critical). It is desirable that the second derivative of the envelope function be everywhere smooth, because of its important role in the minimization procedure, and we therefore decided that all derivatives up to and including the sixth should be continuous. There is no unique solution to this problem, and we chose to use a splined polynomial because the coefficients of such approximants are easily computed with a pocket calculator, and they have computationally simple derivatives. The exact method of calculating such polynomials has already been described elsewhere in a different context (*28*).

The sinc function is even, and its envelope, sincenv, is consequently also symmetric about the origin, which might lead one to think that a polynomial approximant about the origin must also be even. We did calculate several such approximants, but it turned out to be better to make one of mixed parity and to reflect it at the origin, because this leads to fewer numerical problems and to smaller higher derivatives between the blend points. Indeed, we even chose to use an approximant that actually falls slightly below the central peak of the sinc function for the same reasons, though there is no difficulty finding solutions that are never below the true envelope (see Fig. 5). In our application, this level of approximation to sincenv is more than adequate.

We treat the envelope of $2J_1(v)/v$ in much the same way, except that Bessenv cannot easily be computed to the same degree of accuracy as sincenv. The reason for this is simply that we do not have an accurate analytic form for the envelope in the region of interest. The asymptotic form is normally given as $\pi/2v^{-3/2}$, but this underestimates peaks near to the origin by a few percent. However, this level of accuracy is also more than adequate. The splined polynomial that we use is nowhere less than $2J_1(v)/v$ and osculates with $\pi/2v^{-3/2}$ at $v = 3\pi/2$ (see Fig. 6). The position of this blend point is also not critical, and it was chosen on the basis of well-controlled higher derivatives of the resulting polynomial.

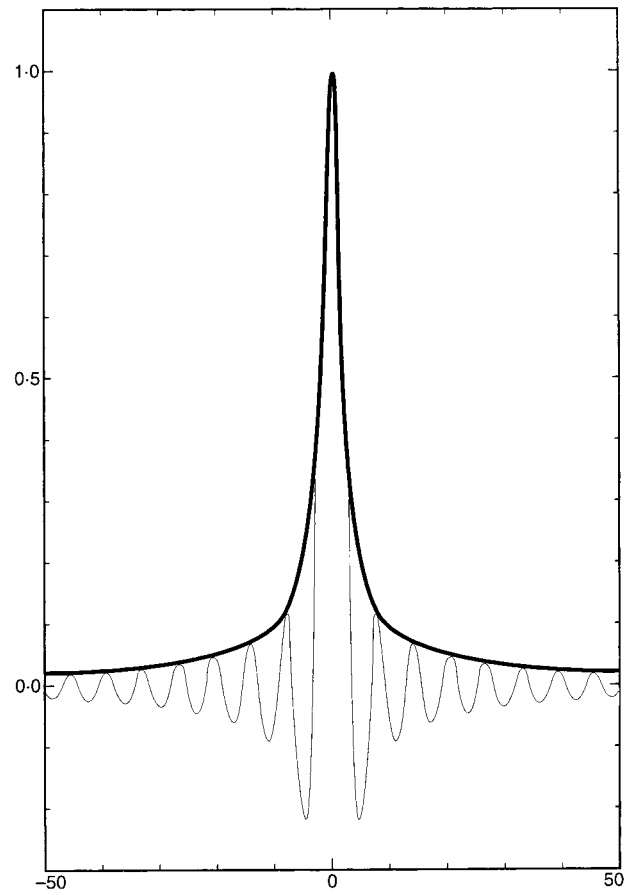

FIG. 5. The sincenv function. The envelope over the sinc function representing residual signal amplitudes in the *Z*-direction.

APPENDIX A2

The Method of Minimization

It is fortunate that in our method the total penalty function to be minimized is very smooth and has a known analytic form. The first and second derivatives necessary for an efficient minimization based on the method of Raphson and Newton are also smooth and calculable without approximation: indeed, the approximations Bessenv and sincenv were deliberately calculated with the smoothness of their second derivatives in mind.

It is a basic and useful property of a stationary point in any number of dimensions that the slope of the function being considered is zero. Minima are a special class of stationary point having the additional property that the local curvature is unconditionally positive with respect to any small changes in any of the free parameters. This means that the matrix of second derivatives (referred to here as the Hessian matrix) can be expected to be positive definite at the minimum that we are seeking. The Hessian matrix also gives us the possibility of identifying other types of stationary points, i.e., saddle points and maxima, though, importantly, it cannot distinguish a local from a global minimum.

In the method of Raphson and Newton, which can be considered for most practical purposes to be the most efficient means of finding the zero-crossing point of a (scalar) function of a single variable, an improved estimate of the solution, say a', is found by substituting iteratively the current best estimate of the solution, say a, into the assignment: $a' \leftarrow a - [f'(a)]^{-1} f(a)$, where $f'(a)$ is the first derivative of f with respect to its argument at a (*27*). This method applies without

modification to vector functions of an arbitrary number of parameters, so long as $[f']^{-1}$ is taken to mean when necessary a generalized matrix inverse (*21, 22, 24–26*) since f' may be a nonsquare matrix. In the present application, all that we need to do is to replace a by our free parameters t^X, t^Y, t^Z arranged in a linear (vector-like) array, and replace f by the gradient of the penalty function, i.e., $\nabla_t(N + P)$, which we call the Jacobian matrix. The derivative function f' in the method of Raphson and Newton becomes the curvature, i.e., the Hessian matrix of second derivatives of the combined penalty function, so the iteration becomes

$$t' \leftarrow t - [\nabla_t^2(N + P)]^{-1}\nabla_t(N + P). \qquad [A2.1]$$

This iteration achieves quadratic (i.e., rather fast) convergence toward any stationary point of ellipsoidal geometry, as assumed implicitly in its derivation because of the use of second derivatives. Slower convergence than might naïvely be expected is sometimes observed. The reason for this is that in free-parameter spaces of higher dimension, the instrumental penalty function and the NMR penalty function combine to form a sum whose minima are curved so that they can have a shape rather like a banana, and are often even more sinuous. In such a situation, even the accurate knowledge that our program has of the local curvature is clearly insufficient to prescribe a rapid path to the minimum. It would be natural to ask whether a minimization taking into account third or higher derivatives might perform better. We have not tried this for two reasons: the first is that the number of derivatives of even a scalar function rises as the number of parameters raised to the order of the derivatives required, meaning a potentially enormous extra computational cost per iteration; the second is that schemes using higher derivatives have a tendency to become unstable, and are thus doubly unattractive.

It is not necessary to evaluate the inverse of the Hessian matrix explicitly, since only its product with the Jacobian is required, and this lesser calculation is performed reliably by the elegant and widely accepted conjugate gradient algorithm (*20*).

The curvature of the instrumental penalty function, P, is positive everywhere inside the bounding divergences (see Fig. 7), which causes no problems. However, the NMR penalty function N, being a sum of envelope functions crossing in many different directions, has a unique maximum at the origin of wavevector space, and an indefinite number of saddle points.

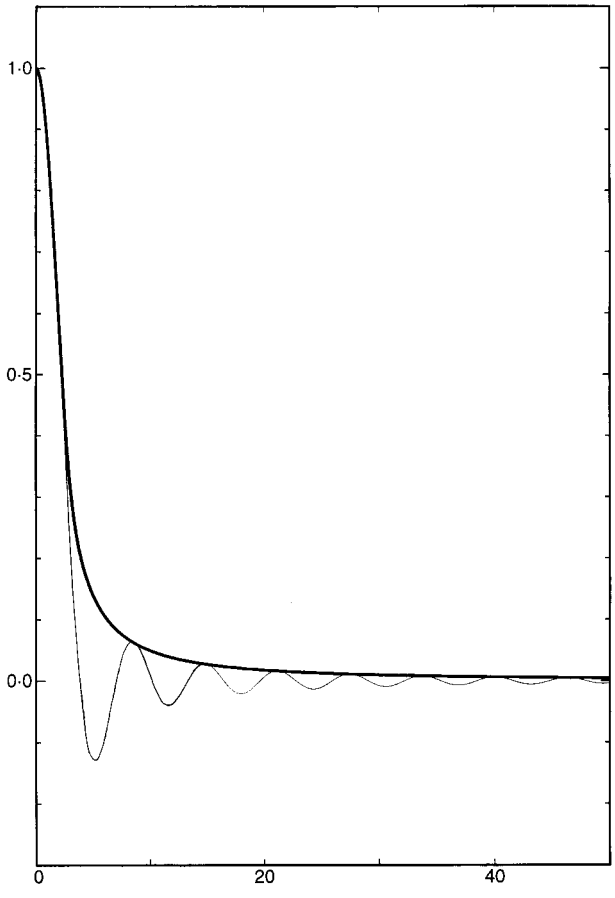

FIG. 6. The Bessenv function. The approximate envelope over the $2J_1(v)/v$ function representing residual signal amplitudes in the XY-plane.

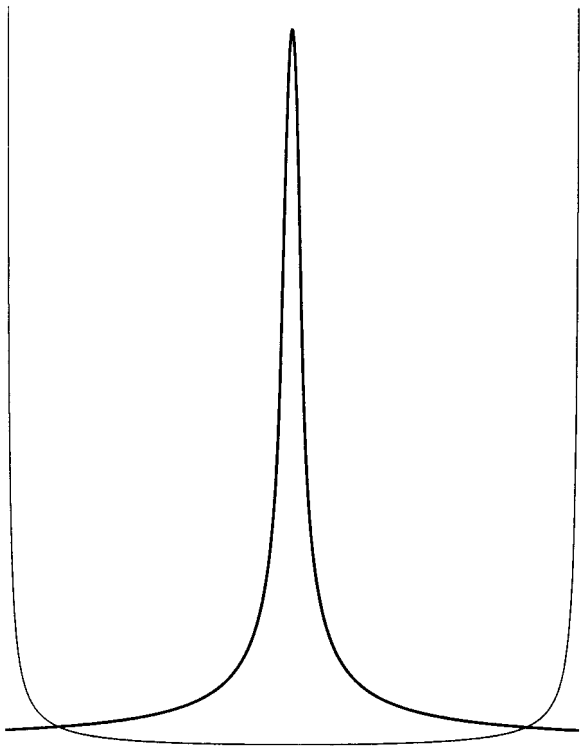

FIG. 7. The instrumental penalty function. This function rises smoothly to infinity at the maximum achievable field gradient in a given direction. It is represented figuratively with the sincenv function, though in fact they are specified in different spaces displayed with coincident origins.

If no action were taken to avoid it, these could all act as attractors if Eq. [A2.1] were used as it stands. To some extent, the method used to prevent this from happening is arbitrary—one might even say a matter of taste. The method that we have used, with success, is to find the most negative diagonal element of the Hessian matrix, and then if it is actually negative, to subtract its value from the entire diagonal. This is the same as adding a positive multiple of the identity matrix and has the effect of distorting the curvature just sufficiently to prevent any attraction to the nonminimal stationary point. In this way, the algorithm always moves in the downhill direction. It has turned out to be necessary in practice to limit the amount by which the diagonal of the Hessian may be loaded, to prevent numerical overflows in the conjugate gradient routine. In cases where the saddle point curvature is more extreme, the algorithm simply steps a fixed distance along the vector represented by the Jacobian. It is rare for this action to occur more than once per minimization.

It can happen that the curvature represented by the Hessian is so small that the calculated change in the free parameters would place them outside of the allowed region. To prevent this from happening, the length of the vector representing the change is modified by a formula based on the hyperbolic tangent. This has the property of leaving small changes unaltered, since the function has unit slope at the origin, but limits large changes to some preset value.

Though the mathematical properties of the total penalty function per se are unexceptionable, the differences between its extremal slopes and curvatures are rather large, and it was necessary to be more than usually careful about the computational implementation to prevent floating-point overflows in the conjugate gradient routine.

APPENDIX A3

The Construction of the Gradient Pulse Sequences

We follow earlier work (*12*) and create field-gradient pulse sequences as a linear superposition of allowed profiles or "vectors," represented here as **S.** Allowed profiles are defined as having the property of not reducing the amplitude of signals arising from wanted coherence transfer pathways. It often happens that the number of such vectors exceeds the dimensionality of the space that they span. In the earlier work, this degeneracy was removed by using a Gram–Schmidt algorithm to create a minimal "suppressive" set of orthogonal vectors. We also make use of the Gram–Schmidt algorithm, but we normally keep all of the extra vectors. These have the property (within the level of approximation used throughout this paper) of affecting none of the specified coherence transfer pathways, wanted or unwanted, and are hence called "free." In the earlier work, their inclusion in the analysis would have served no purpose, but once the instrumental limit on the strength of any given gradient pulse is taken into account, then the extra implied degrees of freedom allow the gradient pulse sequence to be adjusted or trimmed to make fuller use of the capabilities of the equipment. As far as the minimization procedure is concerned, it makes little difference whether a given profile belongs to the suppressive or to the free set, and they are consequently grouped together in the form represented here as **S.** We thus write the sequence of field gradient pulses in the *A*-direction as

$$\mathbf{g}_r^A = \sum_i \mathbf{S}_{ri} t_i^A. \qquad [A3.1]$$

In this equation, the t are the free parameters of our analysis, which are varied independently in order to find the minimum of the overall penalty function. There is some freedom of interpretation of notation here. For example, in the minimization routine, it makes sense to think of the parameters t^X, t^Y, t^Z as being arranged in a linear (vector-like) array, whereas they are more correctly interpreted as a set of three independent sequences of identical length, and thus might appear to fit more naturally into matrix notation. However, these interpretations are of only secondary importance, and to prevent the possibility of any confusion, we have retained a full index notation wherever necessary. The set of allowed profiles, **S,** is unproblematic, and it need be noted only that it is a fixed quantity under the minimization and is the same for all three gradient directions; it also always appears in the equations in a position where it can be represented naturally as a matrix.

The minimization is performed with respect to changes in the free parameters, whereas the physical problem depends directly on the individual field-gradient pulses. The two are coupled by the derivatives:

$$\frac{\partial \mathbf{g}_r^A}{\partial t_i^A} = \mathbf{S}_{ri}, \qquad [A3.2]$$

which enter into the equations via the chain rule of the differential calculus. All other derivatives of **g** vanish, whether they be mixed or of higher order.

APPENDIX A4

Minimizing the Instrumental Penalty Function

The Jacobian and Hessian matrices of the instrumental penalty function are computed in a stepwise fashion using the chain rule. We calculate the first derivative with respect to the change in integrated strength of an individual field gradient pulse as

$$\frac{\partial P}{\partial \mathbf{g}} = \frac{c\hat{\mathbf{g}}^4 \mathbf{g}}{(\hat{\mathbf{g}}^2 - \mathbf{g}^2)^2}. \qquad [A4.1]$$

It will be noticed immediately that the sum in Eq. [3.2] has vanished. This is because the **g** here refers to a single gradient pulse, and only the term under the summation with the same indices survives the differentiation, the others being independent variables. The second derivative with respect to the same integrated field gradient pulse strength is then given by

$$\frac{\partial^2 P}{\partial \mathbf{g}^2} = \frac{c\hat{\mathbf{g}}^4}{(\hat{\mathbf{g}}^2 - \mathbf{g}^2)^2} + \frac{4c\hat{\mathbf{g}}^4\mathbf{g}^2}{(\hat{\mathbf{g}}^2 - \mathbf{g}^2)^3}. \qquad [A4.2]$$

It is now possible to see why P has the form that it does, for if $\mathbf{g} \leftarrow 0$, then $\partial^2 P/\partial \mathbf{g}^2 = c$, the chosen curvature at the origin.

The terms of the Jacobian matrix, here labeled explicitly, are calculated using the chain rule and Eq. [A3.2]:

$$\frac{\partial P}{\partial t_i^A} = \sum_r \frac{\partial \mathbf{g}_r^A}{\partial t_i^A}\frac{\partial P}{\partial \mathbf{g}_r^A} = \sum_r \mathbf{S}_{ri}\frac{\partial P}{\partial \mathbf{g}_r^A}. \qquad [A4.3]$$

The Hessian terms are also calculated in a similar way:

$$\frac{\partial^2 P}{\partial t_i^A \partial t_j^A} = \sum_r \frac{\partial \mathbf{g}_r^A}{\partial t_i^A}\frac{\partial \mathbf{g}_r^A}{\partial t_j^A}\frac{\partial^2 P}{\partial \mathbf{g}_r^{A2}} = \sum_r \mathbf{S}_{ri}\mathbf{S}_{rj}\frac{\partial^2 P}{\partial \mathbf{g}_r^{A2}}. \qquad [A4.4]$$

This formula may appear simpler than might be expected, and indeed is so. The reason is that **g,** being linear, has no second derivatives, so that the additional terms generated by taking the derivative of the product in Eq. [A4.3] disappear.

APPENDIX A5

Minimizing the Unwanted NMR Signals

We follow the previously published geometrical description (*12*), in which both the sequence of field gradient pulses in a given direction and the matching composite coherence orders are represented as "vectors." The interaction between them is then represented by the inner product between the two vectors. In our case, since we are considering up to three gradient directions, our gradients themselves become a vector function, and a matrix might be a more appropriate representation for them, the more especially since the result is actually a wavevector. However, the derivatives do not follow a unified structure since they are related to the shape of the specimen, which is assumed to be a cylinder aligned along the Z-axis. This fact largely abolishes any advantage of matrix notation, and we have consequently not adopted it here. We thus write the X-component of the wave-vector (which appertains to the X-gradients) as

$${}_u\mathbf{k}_x = \gamma \mathbf{p}_u \cdot \mathbf{g}^X = \gamma \sum_r \mathbf{p}_{ru} \sum_i \mathbf{S}_{ri} t_i^X \qquad [A5.1]$$

with strictly analogous equations for the Y- and Z-gradients. If matrix notation had been used, these three equations would have been written $\mathbf{k} = \mathbf{g}\mathbf{p}\gamma$, where $\mathbf{k} \equiv ({}_u\mathbf{k}_x,\ {}_u\mathbf{k}_y,\ {}_u\mathbf{k}_z)$.

The cylindrical symmetry of the specimen implies a cylindrical symmetry in its Fourier transform as well, so long as it remains properly centered, as assumed here, and this means that the results cannot depend on azimuthal angle, but only on radius:

$${}_u\mathbf{k}_r = ({}_u\mathbf{k}_x^2 + {}_u\mathbf{k}_y^2)^{1/2}. \qquad [A5.2]$$

The derivatives of this radius are needed for the chain rule used to calculate terms for the minimization and are given by

$$\frac{\partial {}_u\mathbf{k}_r}{\partial {}_u\mathbf{k}_x} = \frac{{}_u\mathbf{k}_x}{{}_u\mathbf{k}_r} \quad \text{and} \quad \frac{\partial {}_u\mathbf{k}_r}{\partial {}_u\mathbf{k}_y} = \frac{{}_u\mathbf{k}_y}{{}_u\mathbf{k}_r}. \qquad [A5.3]$$

As mentioned in the main body of the paper, we make an NMR penalty function to be minimized formed as the sum of an approximate model of the likely amplitudes of all of the unwanted NMR signals, quoted again here in a fuller form:

$$N = \sum_u w_u \,\mathrm{Besselnv}({}_u\mathbf{k}_r R)\,\mathrm{sincenv}({}_u\mathbf{k}_z L). \qquad [A5.4]$$

The fact that we use envelope functions rather than the idealized product in Eq. [2.2] has important consequences. The first is that the overall penalty function is extremely smooth, and we are not trapped by a multitude of zeroes as would happen if Eq. [2.2] were used directly. The second is that the envelope functions are still thought to apply more or less accurately if the sample should depart from ideality in any way, such as being miscentered or not exactly cylindrical.

The terms in the Jacobian matrix derived from Eq. [A5.4] split because of the cylindrical symmetry into ones along the Z-axis,

$$\frac{\partial N}{\partial t_i^Z} = \sum_u \sum_r w_u \,\mathrm{Besselnv}({}_u\mathbf{k}_r R) \times \gamma \mathbf{p}_{ru}\mathbf{S}_{ri} L \left.\frac{\partial\ \mathrm{sincenv}(v)}{\partial v}\right|_{v={}_u\mathbf{k}_z L}. \qquad [A5.5]$$

and ones along the X- and Y-axis,

$$\frac{\partial N}{\partial t_i^X} = \sum_u \sum_r w_u \gamma \mathbf{p}_{ru}\mathbf{S}_{ri}\frac{{}_u\mathbf{k}_x}{{}_u\mathbf{k}_r} R \times \left.\frac{\partial\ \mathrm{Besselnv}(v)}{\partial v}\right|_{v={}_u\mathbf{k}_r R} \mathrm{sincenv}({}_u\mathbf{k}_z L). \qquad [A5.6]$$

Only the equation for the X-axis is given, because the equation for the Y-axis follows the same form.

The split caused by cylindrical symmetry has an increased effect when considering the terms of the Hessian matrix. We have first the pure second derivative along the Z-axis:

$$\frac{\partial^2 N}{\partial t_i^Z \partial t_j^Z} = \sum_u \sum_r \sum_s w_u \,\mathrm{Bessenv}({}_u\mathbf{k}_r R) \times \gamma^2 \mathbf{p}_{ru}\mathbf{p}_{su}\mathbf{S}_{ri}\mathbf{S}_{sj} L^2 \frac{\partial^2 \,\mathrm{sincenv}(v)}{\partial v^2}\bigg|_{v={}_u\mathbf{k}_z L}. \quad [A5.7]$$

There is then the mixed second derivative, when one axis is Z and the other is either X or Y:

$$\frac{\partial^2 N}{\partial t_i^X \partial t_j^Z} = \sum_u \sum_r \sum_s w_u \gamma^2 \mathbf{p}_{ru}\mathbf{S}_{ri} \frac{{}_u\mathbf{k}_x}{{}_u\mathbf{k}_r} R \times \frac{\partial\ \mathrm{Bessenv}(v)}{\partial v}\bigg|_{v={}_u\mathbf{k}_r R} \mathbf{p}_{su}\mathbf{S}_{sj} L \times \frac{\partial\ \mathrm{sincenv}(v)}{\partial v}\bigg|_{v={}_u\mathbf{k}_z L}. \quad [A5.8]$$

Again, the equation referring the Y-axis is not given, since it follows the same form by direct substitution. The pure second derivative with respect to the X is given by

$$\frac{\partial^2 N}{\partial t_i^X \partial t_j^X} = \sum_u \sum_r \sum_s w_u \gamma^2 \mathbf{p}_{ru}\mathbf{p}_{su}\mathbf{S}_{ri}\mathbf{S}_{sj} R \times \left\{ \frac{{}_u\mathbf{k}_x^2}{{}_u\mathbf{k}_r^2} R \frac{\partial^2\ \mathrm{Bessenv}(v)}{\partial v^2}\bigg|_{v={}_u\mathbf{k}_r R} + \frac{{}_u\mathbf{k}_y^2}{{}_u\mathbf{k}_r^3} \frac{\partial\ \mathrm{Bessenv}(v)}{\partial v}\bigg|_{v={}_u\mathbf{k}_r R} \right\} \mathrm{sincenv}({}_u\mathbf{k}_z L), \quad [A5.9]$$

and the equation for the pure second Y-derivative follows by symmetry. Finally, there is the mixed second derivative with respect to the X-axis and Y-axis:

$$\frac{\partial^2 N}{\partial t_i^X \partial t_j^Y} = \sum_u \sum_r \sum_s w_u \gamma^2 \mathbf{p}_{ru}\mathbf{p}_{su}\mathbf{S}_{ri}\mathbf{S}_{sj} \frac{{}_u\mathbf{k}_{xu}\mathbf{k}_y}{{}_u\mathbf{k}_r^2} R \times \left\{ R \frac{\partial^2\ \mathrm{Bessenv}(v)}{\partial v^2}\bigg|_{v={}_u\mathbf{k}_r R} - \frac{1}{{}_u\mathbf{k}_r} \frac{\partial\ \mathrm{Bessenv}(v)}{\partial v}\bigg|_{v={}_u\mathbf{k}_r R} \right\} \mathrm{sincenv}({}_u\mathbf{k}_z L). \quad [A5.10]$$

APPENDIX A6: NOMENCLATURE

A	an axis, i.e., X, Y or Z
$\mathbf{B}$	a magnetic field
Bessenv	an approximation to the envelope of the function $2J_1(v)/v$
c	the curvature at the origin of the instrumental penalty function
f	the time profile of a pulsed field gradient
F	the number of free precession periods
$\mathbf{g}$	an array of pulsed field-gradient strengths representing a pulse sequence
$\mathbf{g}^X$	an array of field X-gradient pulse strengths; similarly $\mathbf{g}^Y$, $\mathbf{g}^Z$
$\hat{\mathbf{g}}$	the maximum permitted strength of a gradient pulse
i, j	indices to a free parameter
J	a Bessel function of the first kind (*23*)
L	the length of the sample, assumed cylindrical
N	a penalty function representing unwanted NMR signals
r, s	indices to a pulse within a sequence
P	a penalty function representing instrumental limitations
$\mathbf{p}$	an array of composite coherence orders
R	the radius of the sample, assumed cylindrical
$\mathbf{k}_r$	the radial component of a wavevector (i.e., in the X, Y-plane)
${}_u\mathbf{k}_r$	the radial component of a wavevector relating to pathway u
$\mathbf{S}$	a set of allowable gradient pulse sequences
sinc	the $\mathrm{sinc}(v) = \sin(v)/v$ function
sincenv	an approximation to the envelope of the sinc function
t	a free parameter
t^X	a free parameter varying gradients along the X-axis; similarly t^Y, t^Z
τ	time
u	an index denoting an unwanted coherence transfer pathway
v	a general scalar argument
w	a weighting factor for a given unwanted coherence transfer pathway
${}_u\mathbf{k}_x$	the component along the X-direction of a wavevector relating to pathway u; similarly ${}_u\mathbf{k}_y$, ${}_u\mathbf{k}_z$
X, Y	the X- and Y-axes (across the Zeeman field)
Z	the Z-axis (along the Zeeman field)
$\mathbf{k}_z$	the component of a wavevector along the Z-direction
γ	a gyromagnetic ratio (usually of the proton)
σ	an approximation to the expected amplitude of an NMR signal

REFERENCES

1. A. Wokaun and R. R. Ernst, Selective detection of multiple quantum transitions in NMR by two-dimensional spectroscopy, *Chem. Phys. Lett.* **52,** 407–412 (1977).
2. A. D. Bain, Coherence levels and coherence pathways in NMR. A simple way to design phase cycling procedures, *J. Magn. Reson.* **56,** 418–427 (1984).
3. G. Bodenhausen, H. Kogler, and R. R. Ernst, Selection of coherence-transfer pathways in NMR pulse experiments, *J. Magn. Reson.* **58,** 370–388 (1984).
4. A. A. Maudsley, A. Wokaun, and R. R. Ernst, Coherence transfer echoes, *Chem. Phys. Lett.* **55,** 9–14 (1978).
5. A. Bax, P. G. DeJong, A. F. Mehlkopf, and J. Smidt, Separation of the different orders of NMR multiple-quantum transitions by the use of pulsed field gradients, *Chem. Phys. Lett.* **69,** 567–570 (1980).
6. J. Keeler, R. T. Clowes, A. L. Davis, and E. D. Laue, Pulsed-field gradients: theory and practice, *in* "Methods in Enzymology," Vol. 239 (N. J. Oppenheimer and T. L. James, Eds.), pp. 145–207, Academic Press, San Diego, and references therein (1994).
7. R. E. Hurd, Gradient-enhanced spectroscopy, *J. Magn. Reson.* **87,** 422–428 (1990).
8. G. E. Vuister, R. Boelens, R. Kaptein, R. E. Hurd, B. John, and P. C. M. van Zijl, Gradient-enhanced HMQC and HSQC spectroscopy. Applications to ^{15}N labeled Mnt repressor, *J. Am. Chem. Soc.* **113,** 9688–9690 (1991).
9. J. Ruiz-Cabello, G. W. Vuister, C. T. W. Moonen, P. van Gelderen, J. S. Cohen, and P. C. M. van Zijl, Gradient-enhanced heteronuclear correlation spectroscopy. Theory and experimental aspects, *J. Magn. Reson.* **100,** 282–302 (1992).
10. A. Ross, M. Czisch, C. Cieslar, and T. A. Holak, Efficient methods for obtaining phase-sensitive gradient-enhanced HMQC spectra, *J. Biomol. NMR* **3,** 215–224 (1993).
11. A. L. Davis, E. D. Laue, J. Keeler, D. Moskau, and J. Lohman, Absorption-mode two-dimensional NMR spectra recorded using pulsed field gradients, *J. Magn. Reson.* **94,** 637–644 (1991).
12. L. Mitschang, H. Ponstingl, D. Grindrod, and H. Oschkinat, Geometrical representation of coherence transfer selection by pulsed field gradients in high-resolution nuclear magnetic resonance, *J. Chem. Phys.* **102,** 3089–3098 (1995).
13. L. Mitschang, Signal selection in high-resolution NMR by pulsed field gradients: I. Geometrical analysis, *J. Magn. Reson.,* this issue.
14. A. Sommerfeld, "Partielle Differentialgleichungen der Physik," Verlag Harri Deutsch, Frankfurt am Main (1978).
15. B. K. John, D. Plant, S. L. Heald, and R. E. Hurd, Efficient detection of C_αH–HN correlations in proteins using gradient enhanced ^{15}N HMQC-TOCSY, *J. Magn. Reson.* **94,** 664–669 (1991).
16. P. R. Halmos, "Finite-Dimensional Vector Spaces," Springer Verlag, New York (1974).
17. H. Kessler, P. Schmieder, and H. Oschkinat, 3D heteronuclear nuclear-magnetic-resonance techniques for ^{13}C in natural abundance, *J. Am. Chem. Soc.* **112,** 8599–8600 (1990).
18. J. M. Schmidt and H. Rüterjans, Proton-detected 2D heteronuclear shift correlation via multiple-quantum coherences of the type I_2S, *J. Am. Chem. Soc.* **112,** 1279–1280 (1990).
19. J. Keeler and D. Neuhaus, Comparison and evaluation of methods for two-dimensional NMR spectra with absorption-mode lineshapes, *J. Magn. Reson.* **63,** 454–472 (1985).
20. M. R. Hestenes and E. Stiefel, Methods of conjugate gradients for solving linear systems, *J. Res. Nat. Bureau Standards* **49,** 409–436 (1952).
21. E. H. Moore, On the reciprocal of the general algebraic matrix [abstract], *Bull. Amer. Math. Soc.* **26,** 394–395 (1920).
22. E. H. Moore, "General Analysis," American Philosophical Society, Philadelphia (1935).
23. F. W. J. Olver, Section 9.1, Bessel Functions of Integer Order, *in* "Handbook of Mathematical Functions" (M. Abramowitz and I. A. Stegun, Eds.), pp. 355–433, Dover, New York (1965).
24. R. Penrose, A generalized inverse for matrices, *Proc. Cambridge Phil. Soc.* **51,** 406–413 (1955).
25. G. Peters and J. H. Wilkinson, The least squares problem and pseudo-inverses, *Computer J.* **13,** 309–316 (1970).
26. C. R. Rao and S. K. Mitra, Preface (pp. vii–ix) *in* "Generalized Inverse of Matrices and Its Applications," Wiley, New York (1971).
27. K. F. Riley, "Mathematical Methods for the Physical Sciences," pp. 303–305, Cambridge University Press, London (1974).
28. D. J. Thomas, The graduation of secondary structure elements, *J. Mol. Graphics* **12,** 146–152 (1994).
29. D. J. Thomas, Calibrating an area-detector diffractometer: Imaging geometry, *Proc. R. Soc. Lond. A* **425,** 129–167 (1989).
30. G. L. Shaw, T. Müller, H. R. Mott, H. Oschkinat, I. D. Campbell, and L. Mitschang, Constant-time HQQC experiment for protein NMR spectroscopy, *J. Magn. Reson.* **124,** 479–483 (1997).
31. J. Körger, H. Pfeiffer, and W. Heink, Principles and applications of self-diffusion measurements by NMR, *Adv. Magn. Reson.* **12,** 1–89 (1988).
32. P. C. M. van Zijl, M. O'Neil Johnson, S. Mori, and R. E. Hurd, Magic-angle-gradient double-quantum-filtered COSY, *J. Magn. Reson.* **A113,** 265–270 (1995).
33. Q. He, W. Richter, S. Vathyam, and W. S. Warren, Intermolecular multiple-quantum coherences and cross correlations, in solution nuclear magnetic resonance, *J. Chem. Phys.* **98,** 6779–6800 (1993).
34. M. H. Levitt, Demagnetization field effects in two-dimensional solution NMR, *Concepts Mag. Reson.* **8,** 77–103 (1996).
35. P. Broekaert, A. Vlassenbroek, J. Jeener, G. Lippens, and J.-M. Wieruszeski, Observation and selective supression of the dipolar-field effects in 2D NMR in Liquids in Homogeneous Fields, *J. Magn. Reson. A* **120,** 97–104 (1996).
36. A. Vlassenbroek, J. Jeener, and P. Broekaert, Macroscopic and microscopic fields in high-resolution liquid NMR, *J. Magn. Reson. A* **118,** 234–246 (1996).
37. P. C. M. van Zijl, and C. T. W. Moonen, *in* "NMR, Basic Principles and Progress" (J. Seelig and M. Rudin, Eds.), Vol. 26, p. 67, Springer Verlag, Berlin (1992).